LAWRENCE
LIVERMORE
NATIONAL
LABORATORY

UCRL-JRNL-227861

Gryrokinetic Simulations of ETG and ITG Turbulence

A. M. Dimits, W. M. Nevins, D. E. Shumaker, G. W. Hammett, T. Dannert, F. Jenko, W. Dorland, J. N. Leboeuf, T. L. Rhodes, J. Candy, C. Estrada-Mila

February 7, 2007

Nuclear Fusion

Disclaimer

Gyrokinetic Simulations of ETG and ITG Turbulence*

A M Dimits[1], W M Nevins[1], D E Shumaker[1], G W Hammett[2], T Dannert[3], F Jenko[3], W Dorland[4], J N Leboeuf[5], T L Rhodes[5], J Candy[6] and C Estrada-Mila[7]

[1]Lawrence Livermore National Laboratory, USA
[2]Princeton Plasma Physics Laboratory, USA
[3]Max Planck Institut fur Plasmaphysik, Germany
[4]University of Maryland, USA
[5]University of California, Los Angeles, USA
[6]General Atomics, San Diego, USA
[7]University of California, San Diego, USA

e-mail contact of main author: dimits1@llnl.gov

Abstract: We have carried out an investigation, using PIC- and continuum-gyrokinetic-code simulations and analytical theory, of a significant discrepancy between published continuum-code simulations and subsequent global particle-in-cell (PIC) simulations of electron-temperature-gradient (ETG) turbulence. This investigation strongly supports the conclusion from the earlier continuum-code simulations that ETG turbulence can drive the electron thermal conductivity χ_e large enough to be significant in some tokamaks. A successful ETG-turbulence benchmark between PIC and continuum codes for ETG turbulence has also been completed. Scans in the magnetic shear show an abrupt transition to a high-χ_e state as the shear is increased from the benchmark value of s=0.1 to above s=0.4. When nonadiabatic ions are used, this abrupt transition is absent, and χ_e reaches values consistent with transport analyses of DIII-D, JET, and JT60-U discharges. The balances of zonal-flow driving and damping terms in late-time quasi-steady phase of ITG turbulence have been unfolded using a new run-time gyrokinetic-simulation diagnostic. The driving is found to be mostly by the Reynolds' stress, while the dissipation is mostly by the linear (transit-time) damping terms. It is also shown that useful zonal-flow-balance information can be obtained with spatially localized samples at as few as four poloidal locations. Real-geometry simulations have been undertaken, using the nonlinear δf-PIC gyrokinetic code PG3EQ_NC, of the DIII-D "Cyclone" shot #81499 and of shot #118561, which had broad wavenumber range density fluctuation measurements. Real geometry is found to have a significant effect on the transport rates, even though the effect on the linear growth rates is often modest.

PACS codes: 52.65.Tt, 52.35.Ra, 52.25.Fi

1. Introduction

We report progress in nonlinear gyrokinetic simulation of toroidal electron-temperature-gradient (ETG) and ion-temperature-gradient (ITG) turbulence.

Gyrokinetic continuum-code simulations of ETG turbulence have indicated a sufficiently large value of the electron thermal conductivity χ_e to be potentially significant in tokamaks [1]. This was cast into doubt by more recent particle-in-cell (PIC) simulations [2] which, using similar plasma parameters, gave significantly lower values of χ_e. The differences between [1] and [2] were attributed to insufficient phase-space resolution and novel physics associated with global geometry [2]. Ref. [1] also differs from [2] in that magnetically trapped particles are eliminated in [1] ($r/R = 0$, where r and R are respectively the minor and major radii), but retained in [2] ($r/R = 0.18$). In section 2, we summarize investigations that we have carried out [3,4], using gyrokinetic simulations complemented by analytical theory, of the above discrepancy and the proposed explanations, and of the general question of whether ETG turbulence can be important in tokamaks.

Anomalous ion thermal transport in some tokamak discharges [5] is believed to be caused by the toroidal ITG and related turbulence. There is now widespread evidence from simulations (see e.g., Refs. [6], [7], and [8]) that zonal flows are a key component in the dynamics of such turbulence. For example, differences in zonal-flow dynamics account for the large difference in normalized (to gyroBohm) transport values between ITG and ETG turbulence [1]. Several studies to date have addressed the generation of zonal flows in the early nonlinear phase [9] of ITG turbulence, and the stability of idealized zonal-flow states [10]. However, information on the relative importance of different driving and damping mechanisms in the in the late-time quasi-steady state would greatly add to the understanding the turbulence-zonal-flow system, and is directly accessible in simulations. We have therefore developed a run-time gyrokinetic-simulation diagnostic to extract this information and which has enabled us to unfold the balances of zonal-flow driving and damping terms in late-time quasi-steady ITG turbulence. This diagnostic and its application are discussed in section 3.

Our zonal-flow-balance diagnostic is similar in approach to work by B. Scott [11] and by K. Hallatschek *et al.* [12]. Scott addressed zonal flows in electromagnetic drift turbulence using with a decomposition of the sources and sinks of zonal flow both by physical term and wavenumber. Our diagnostic is integral in wavenumber. A wavenumber decomposition of the sources and sinks in our ITG and ETG simulations will be presented in future work. Hallatschek *et al.* [12] examined zonal flow sources and sinks in drift wave turbulence with a real-space diagnostic which is similar in spirit to ours, but uses a further decomposition of the zonal fields into a zero-frequency modal component and a geodesic-acoustic-mode (GAM) component. An approximate analogue of this diagnostic may be possible for our kinetic simulations, but is less straightforward than for the fluid system considered in Ref. [12]. That work also focused on terms that were useful for the idendification of a $V_{\shortparallel}$' instability as the mechanism for tertiary instability of the zonal flows in the edge-related regime considered there.

Real tokamak discharge cross sections have significant departures from circularity due to intentional distortions (e.g., elongation and triangularity), and the presence of divertor X points. This has motivated the development of a real-geometry versions of gyrokinetic simulation codes. We have therefore developed SUMMIT/PG3EQ_NC, a real-geometry versions of the gyrokinetic code PG3EQ. Some results of applications of SUMMIT/PG3EQ_NC are presented in section 4.

Conclusions and discussion of the results of this work are presented in section 5.

2. ETG Turbulence

Simulations were carried out using the flux-tube gyrokinetic δf -PIC code, PG3EQ [8], using the same physical parameters as in [2] and [13], as well as with $r/R = 0$. (We will refer to these parameters as "Cyclone-like," since they match those used in the "Cyclone" study reported in Ref. [13]). Both sets of simulations reproduce the key features of the results reported in [2] including (1) the first nonlinear-saturation peak in χ_e, (2) the rise after this peak shown in Fig. 4 of Ref. [2], (3) the low late-time value of χ_e ($\chi_e \approx 3\chi_{eGB}$ for $r/R = 0.18$ and $\chi_e \approx 1.5\chi_{eGB}$ for $r/R = 0$, where $\chi_{eGB}=v_{te}\,\rho_e^2/L_{Te}$ is the electron "gyroBohm" conductivity), and (4) the downshift in wave number of the nonlinear spectrum relative to the linear spectrum [2]. Thus, global effects are eliminated as the cause of the discrepancy between [1] and [2]. The presence of trapped particles does not significantly change the time dependence of χ_e nor its value in the late-time low-χ_e state.

We have shown [3], however, that in this low-χ_e state in both these PG3EQ simulations and those reported in [2], discrete particle noise has become large enough to suppress the ETG turbulence. Since discrete particle noise is a numerical artifact, it cannot be inferred on the basis of the PIC simulations of Ref. [2] that the higher χ_e values given by the continuum–code simulations of Ref. [1] are incorrect. Note that this conclusion holds for simulations using the Cyclone-like parameters of Refs.

[13], and is expected (see below and Ref. [4]) to hold over a range of magnetic shear values ($0.4 \le S \le S_{\max}$, where $S_{\max} > 0.8$) for the Cyclone value of the temperature gradient (R/L_T=6.9 and greater).

Parker et. al [14] have found that for lower values of the temperature gradient ($5.3 \le R/L_T \le 6.1$), there appears to be a "nonlinear upshift" regime in which the zonal flows grow to suppress the turbulence, as was the case for ITG simulations [13]. However, Lin et al., [14] found much slower growth of and less turbulence suppression by the zonal flows for this case, and investigations are underway to attempt to corroborate one or other of these results.

The demonstration that the late-time low-χ_e state in the δf-PIC Cyclone-like ETG simulations is a result of discrete particle noise was facilitated by the development of a theoretical model of the interaction of δf-PIC simulation noise and physical turbulence [3]. This model reproduces the behavior of noise-affected gyrokinetic δf-PIC simulations of both ETG turbulence, in which the noise suppresses the turbulence, and ITG turbulence, where the noise and turbulence coexist and both contribute to the net transport. A key component of this model is a detailed theoretical result for the spectrum of electrostatic potential noise fluctuations in a δf gyrokinetic particle simulation. This result is based on Krommes' calculation of the gyrokinetic noise spectrum [15], extended to include the effects of numerical filtering, finite-size and weighted particles. Spectra from the late-time, low-χ_e phase of the Cyclone-like δf-PIC ETG simulations show excellent agreement with this noise-based result, indicating that at that time, these simulations are dominated by noise.

The theoretical model predicts that the simulation noise can either suppress the turbulence and result in greatly reduced transport, as it does in the ETG simulations of Refs. [2] and [3], or it can result in enhanced net (physical + noise-driven) transport, as it does in the lowest-particle-number ITG simulations of those shown in Ref. [13]. In the ETG simulations of Refs. [2] and [3], the high degree of anisotropy of the ETG turbulence in the plane perpendicular to the magnetic field ***B*** results in large physical transport levels (normalized to the electron gyroBohm level), as a result of which, the noise grows rapidly to a level where the ExB diffusion it causes is sufficient to stabilize and quench the ETG turbulence. This contrasts with the case of ITG turbulence, for which the much greater isotropy and lower associated physical transport levels (normalized to the respective ion gyroBohm units) results in a much slower buildup of the simulation noise. For the ITG simulations, sufficient particles can quite easily be brought to bear so that the noise-driven diffusion does not significantly the physical turbulence. For smaller particle numbers, the noise driven diffusion can either gradually suppress the net transport or else can result in a net transport increase, as shown in Ref. [13].

We have also shown directly [3] that simulation noise can reduce the linear growth of or completely stabilize the physically unstable ETG modes, strongly suggesting that this stabilization is the cause of suppression of the turbulent transport in the δf-PIC Cyclone-like ETG simulations. This is supported by further analysis, which shows that the time of maximum amplitude of each mode coincides with the time at which its linear growth rate, as modified by the noise diffusion, goes from positive to negative.

Confidence in the ability of gyrokinetic simulations as a tool for understanding and predicting ETG-driven transport was established through a successful inter-code benchmark [4] involving the continuum gyrokinetic codes GYRO [16], GS2 [1], and GENE [1], and the δf-PIC code PG3EQ [8]. Because our attempts to benchmark at the plasma parameters used in [2] produced very large, intermittent transport and strong sensitivity of the results to numerical parameters, we undertook the benchmarks at an alternate reference point, magnetic shear $s = 0.1$ instead of $s = 0.796$. This change produces a large (two orders of magnitude) drop in the heat transport even though the change in the linear growth spectrum is modest. Good agreement was achieved, with the time-interval weighted standard deviation in $\langle \chi_e \rangle$ between codes yielding an error in our estimate of the mean of less than 10%. This agreement between codes is better than that achieved in the Cyclone ITG benchmarking

exercise [13]. Additionally, it was found that the intensity of the ETG turbulent fluctuations, the mean squared ExB velocity shear, as well as the binormal and radial correlation functions is substantially the same between the codes.

Scans in the magnetic shear show that as the magnetic shear is increased over the range $0.1 \le s \le 0.35$ there is an initial large-heat-flux transient, which becomes more dramatic while the late-time ($t > 1500\ L_T/v_{te}$ for GYRO simulations and $t > 2500\ L_T/v_{te}$ for GENE simulations) average of χ_e remains substantially unchanged, varying between 2.7 and $3.8\ (\rho_e/L_T)\rho_e v_{te}$. When the magnetic shear is increased further to $s=0.4$ the electron thermal conductivity takes a dramatic jump to $\langle\chi_e\rangle = O(100) \times (\rho_e/L_T)\rho_e v_{te}$. In simulations with PG3EQ at s=0.4 the heat flux rises to track the results from GYRO and GENE before simulation noise suppresses the turbulence. An indication of problems with these extremely large-χ_e states is that the turbulent fluctuation spectrum becomes nearly monochromatic in binormal wavenumber, dominated by the lowest nonzero-wavenumber mode.

The magnetic shear scan was repeated, employing GYRO, with the adiabatic ions replaced by full gyro-kinetic ions at a mass ratio of $m_i/m_e=400$, and a somewhat larger flux-tube cross-section, $256\rho_e \times 128\rho_e$. (More recently, runs with larger mass ratios have been completed [17]. With kinetic ions the intensity of the initial burst of turbulence increases with increasing magnetic shear. However the electron heat flux drops back down to a modest late-time average value, in the range of 10-14 $\chi_{e,GB}$.

Transport analyses of DIII-D [18], JET [19], and JT-60U [20] discharges suggest that ETG turbulence may be responsible for the electron heat transport across thermal barriers and in the L-mode edge of discharges with internal transport barriers. For example, in the DIII-D discharges analyzed in Ref. [18], the experimental electron heat transport normalized to $\chi_{e,GB}$ was found to be less than 1 in the internal transport barriers and of order 10 in the L-mode edge region, consistent with our ETG simulation results (with kinetic ions) at high magnetic shear. Within the internal transport barrier $\chi_e/\chi_{e,GB}$ is less than or of the order of one, rising to values of less than or about 25 in the L-mode plasma outside the barrier. Analysis of NSTX L-mode discharges [21] finds that χ_e is often substantially larger than χ_i, and there are many cases where χ_e is in the range of 5-10 $\chi_{e,GB}$, consistent with our ETG simulation results.

3. ITG turbulence: Sources and Sinks of Zonal flow.

The development of the zonal-flow-balance diagnostic for gyrokinetic simulations (of ITG turbulence) proceeds by writing an equation (accurate to second order in gyroradius) for the rate of change of the zonal-flow ***ExB*** shear V'_{EB}:

$$\frac{\partial V'_{EB}}{\partial t} \propto \frac{\partial \langle n_{gi} \rangle_{fs}}{\partial t} = \left\langle \int B\, d\mu\, dv_{\parallel}\, d\theta\, \frac{\partial \delta f_g (x - \rho\hat{\rho}_x)}{\partial t} \right\rangle_{fs} . \qquad (1)$$

Here, n_{gi} is the gyrocenter density δf_g is the perturbed gyrocenter distribution, t is the time, B is the magnetic field, μ is the magnetic moment, $v_{\parallel}$ is the parallel velocity, θ is the gyrophase angle, x is the real-space radial position, ρ is the gyroradius and $\hat{\rho}$ is the gyroradius unit vector, and $\langle\ \rangle_{fs}$ denotes a flux surface average. Note that this relationship is accurate to second order in the gyroradius, as are typical finite-Larmor-radius fluid models (e.g., that of Ref. [22]. Higher order terms could be kept if desired either by the insertion of a suitable Pade-based operator (which can be implemented using tridiagonal matrix inversions, as is already done in the zonal field-solver in the PG3EQ code [8]), or simply by viewing
$\langle n_{gi} \rangle_{fs}$ as a useful generalized vorticity quantity whose 9nonlocal) functional dependence on ϕ includes only second and higher even powers. Upon replacement of $\partial \delta f_g / \partial t$ using the nonlinear

gyrokinetic equation [23, 8], each term therein yields a contribution to $\partial V'_{EB}/\partial t$ that can be identified as a source or sink of zonal flow shear.

The terms associated with the radial gyroaveraged ExB drift flow $\bar{V}_{EBx}$ can be further decomposed. Thus,

$$\frac{\partial}{\partial x}\langle \int B\, d\mu\, dv_{\|}\, d\theta\, V_{EBgx}\, \delta f_g(x-\rho\hat{\rho}_x)\rangle_{fs},$$

where V_{EBgx} is the radial ExB drift at the gyrocenter, can be identified as the Reynolds stress. The related term

$$\frac{\partial}{\partial x}\langle \int B\, d\mu\, dv_{\|}\, d\theta\, (\bar{V}_{EBx}-V_{EBgx})\delta f_g(x-\rho\hat{\rho}_x)\rangle_{fs},$$

where $\bar{V}_{EBx}$ is the gyroaveraged radial ExB drift, can be identified with the diamagnetic Reynolds stress [24, 25]. There are several linear terms. One class of terms can be viewed as the divergences of the perturbed ∇B and curvature-drift flows (magnetic pumping) or (with the addition of appropriate magnetization currents) as perturbed diamagnetic and neoclassical fluid flows

$$\frac{\partial}{\partial x}\langle \int B\, d\mu\, dv_{\|}\, d\theta\, (V_{\nabla Bx}+V_{cx})\delta f_g(x-\rho\hat{\rho}_x)\rangle_{fs}$$

where $V_{\nabla Bx}$ and V_{cx} are the radial components of the ∇B and curvature drifts. Additionally, there are terms that represent the change in gyrocenter density associated with ∇B and curvature drifts in the direction of the electric field:

$$\frac{\partial}{\partial x}\langle \int B\, d\mu\, dv_{\|}\, d\theta\, (V_{\nabla B}+V_c).\nabla\phi(x-\rho\hat{\rho}_x)\, F_M\rangle_{fs},$$

where f is the electrostatic potential, and F_M is the equilibrium distribution. These terms are nonzero as a result of the velocity dependences of the ∇B and curvature drift flows. The above decomposition results in an equation of the form

$$\frac{\partial V'_{EB}}{\partial t} \simeq \sum_i R_i\,. \qquad (2)$$

To facilitate analysis, it is helpful to recast this as an equation for a positive definite scalar quantity. One choice is $\langle |V'_{EB}|^2\rangle_x$, the enstrophy associated with the zonal ExB flow. The resulting equation is

$$\frac{\partial\langle |V'_{EB}|^2\rangle_x}{\partial t} \simeq 2\sum_i \langle R_i\, V'_{EB}\rangle_x. \qquad (3)$$

Alternatively, the zonal-flow energy $\langle |V_{EB}|^2\rangle_x$ can be used. It can be shown that (e.g., it follows rigorously from the exact form of the gyrokinetic Poisson equation or from the Pade approximation used in PG3EQ [8]) that $\langle \phi n_{gi}\rangle_x$ is positive definite. This leads to a useful approximate equation for the zonal-flow energy:

$$\frac{\partial\langle |V_{EB}|^2\rangle_x}{\partial t} \simeq 2\sum_i \langle \phi R_i\,\rangle_x\,. \qquad (4)$$

Each of the R_i's contributes a term in Eq. (3) or (4), and is calculated as a profile on the radial mesh in PG3EQ through suitable "particle deposition" operations. The resulting contributions to $\langle |V'_{EB}|^2 \rangle_x$ in Eq. (3) or $\langle |V_{EB}|^2 \rangle_x$ in Eq. (4) are then calculated as a postprocess using the GKV analysis package [3] (and in addition the profile of δn_{gi} or ϕ.) It has been carefully verified that the resulting terms do indeed satisfy Eq. (2) to good accuracy (i.e., that the accumulated R_i terms add to the directly calculated values of $\partial V'_{EB}/\partial t$ across the x-t plane), and consequently also Eqs. (3) and (4).

Figure 1 shows the results of applying this diagnostic to the calculation of the terms in Eq. (3) for a PG3EQ simulation using the parameters of Ref. [13]. [The results for the terms of Eq. (4) have been plotted and are qualitatively similar to those for Eq. (3).] The Reynolds stress contribution is seen to be positive definite and is the main source of zonal flow shear. The linear terms (the sum of which is the blue curve) act as sinks. The total rate of change of $\langle |V'_{EB}|^2 \rangle_x$ is shown as the black curve, while the green curve is the sum of just the Reynolds stress and linear terms. That the green curve tracks the black curve well indicates that that the Reynolds stress and linear terms capture most of the contribution. The net imbalance in the early time (t=200-300) variation is associated with the initial buildup of the zonal flow. It is clear from the figure that the Reynolds stress and linear damping terms are each much larger than the net rate of change of $\langle |V'_{EB}|^2 \rangle_x$, which is the small residual difference between these two terms.

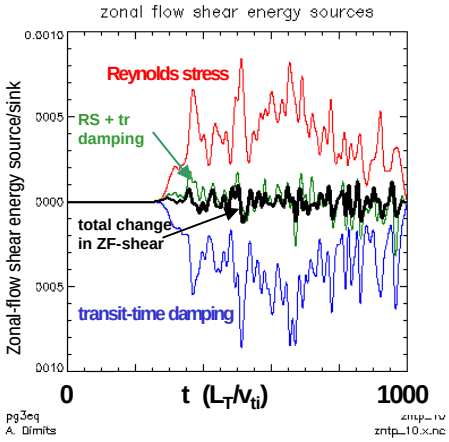

Figure 1. Relative contributions to $\partial \langle |V'_{EB}|^2 \rangle_x / \partial t$ from a PG3EQ simulation using the NTP base case parameters. The red curve is the Reynolds stress, the blue curve is sum of linear terms, the green curve is the sum of the Reynolds stress and linear terms, and the black curve is the total rate of change of $\langle |V'_{EB}|^2 \rangle_x$.

The sources and sinks are further decomposed in figure 2. The diamagnetic Reynolds stress is found to be small, and acts as a weak sink. The linear damping terms have comparable contributions from the magnetic pumping terms and the energy source terms. This diagnostic has been applied to and the same conclusions reached for a variety of PG3EQ simulation cases, including several points in temperature-gradient scans about the Cyclone parameter set and the "NTP" parameter set [26].

We have also extended this analysis to provide guidance for experimental fluctuation diagnostics, which tend to be able to measure fluctuations in a spatially localized region and are unable to diagnose fluctuations over an entire flux surface or even a flux-surface ring spanning a poloidal circuit and a small range of toroidal angle. It is found that 4 poloidally localized samples are sufficient, and appear to be necessary, to provide a resolution of the zonal-flow shear sources and sinks. Figure 3 shows the results of application of the diagnostic using simulation data from only the top, bottom and inboard and outboard midplanes. Attempts have been made with 2 poloidally localized samples at various

poloidal locations. These give traces for the various contributions that do not have a measurably definite sign. Using 8 poloidal samples improves the quality of the time traces of the sources and sinks over 4 samples.

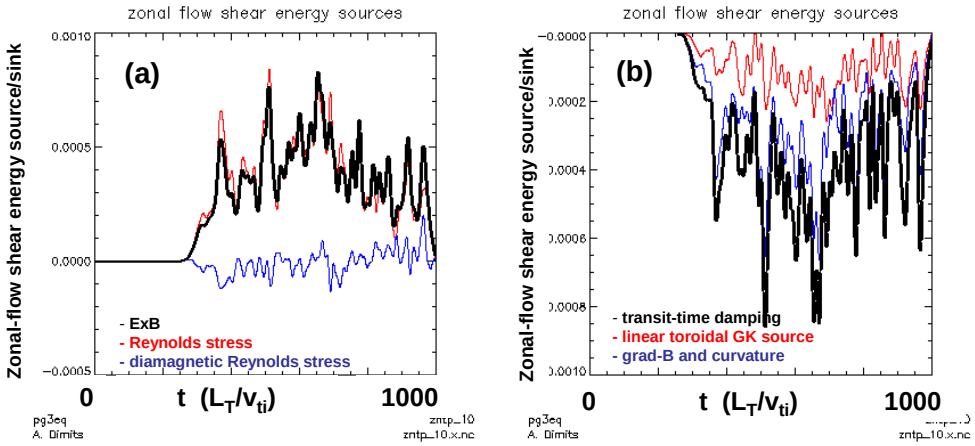

Figure 2. Relative contributions to $\partial\langle|V'_{EB}|^2\rangle_x/\partial t$ from the simulation shown in Fig.1. The left panel shows the sources, while the right panel shows the sinks.

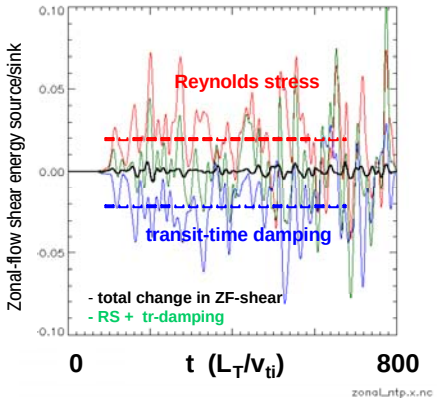

Figure 3. Relative contributions to $\partial\langle|V'_{EB}|^2\rangle_x/\partial t$ from the simulation shown in Fig.1, but with the quantities calculated by sampling at four poloidal locations (outer and inner midplane and top and bottom.

Preliminary results have been obtained from investigations of zonal-flow dynamics and the application of the above diagnostic to ETG turbulence simulations (carried out with PG3EQ). In the Cyclone-like s=0.8 cases in which the transport rises to large values, it has been found that this tendency for χ_e to rise to large values goes away if the zonal potential (***ExB*** flow) is removed. The cause for this counterintuitive result is under investigation. Additionally, restarts during the χ_e rise phase with the zonal potential zeroed out result in a cessation of the rise. Secondly for the s=0.1 benchmark case, which does reach a reasonably robust steady state, the zonal-flow balance dynamics differs significantly from that in ITG simulations. The Reynolds's stress is still found to be a source, but it is compensated by the diamagnetic Reynolds' stress so that the net contribution of the gyroaveraged ExB drift

$$\frac{\partial}{\partial x}\langle\int B\, d\mu\, dv_{\|}\, d\theta\, \bar{V}_{EBx}\, \delta f_g(x-\rho\hat{\rho}_x)\rangle_{fs}$$

is small. Additionally, the compression of the radial ∇B and curvature-drift fluxes acts as a source, while the linear toroidal energy sink term acts as a sink of zonal flow energy and enstrophy. The linear terms negate each other as do the nonlinear terms.

4. ITG turbulence: Real-geometry-tokamak gyrokinetic simulations

SUMMIT/PG3EQ_NC is a nonlinear δf-PIC gyrokinetic code which implements real geometry using the quasi-ballooning representation [8] of the field quantities. It has been interfaced to DIII-D equilibrium analyses from the EFIT [27], ONETWO [28], and PLOTEQ [29] codes.

Verification of PG3EQ_NC has been carried out by comparing it in detail to the earlier circular-cross-section gyrokinetic code PG3EQ [8]. Agreement to roundoff for many time steps, and across different parallel domain decompositions has been obtained when the initial loading and equilibrium are identical.

Real geometry PG3EQ_NC simulations have been undertaken of toroidal ITG instability growth and turbulence using equilibria from several DIII-D shots including shots #81499 and #118561. A "circularized" equilibrium with parameters taken from shot #81499 was used as the basis for the "Cyclone" ITG turbulence simulation comparison [6]. Shot #118561 was part of a recent DIII-D campaign in which broad wavenumber range density fluctuation measurements were performed. This range includes wavenumbers from ~ 0.7 cm^{-1} to 35 cm^{-1} ($k\rho_s \approx 0.2$ - 10), covering the range of ITG, and ETG instabilities. Plasma instabilities were excited by using short duration neutral beam blips to modify the plasma parameters from a low-transport ohmic state. These perturbations modified the background temperature and density as well as the density fluctuation behavior. The measured response to these perturbations varied with wavenumber, supporting the need for broad wavenumber comparisons including both the ITG and ETG range of wavenumbers.

Figure 4 shows the time history of the ion thermal transport and images of the electrostatic potentia ϕ on a poloidal section from the ITG simulations using PG3EQ_NC and equilibria from EFIT and ONETWO analyses for shot #81488 at t=4000ms. These simulations show the expected linear ITG instability growth and saturation. The maximum linear growth rate for the case shown in figure 6 is very close to that for the corresponding circularized case (Fig. 7(a) at r/a=0.5), while the late-time ion thermal transport level is reduced to less than half of that for the circularized case. This case was run with a 128x128 (perpendicular) x 64 mesh, with a perpendicular grid cell size of 0.9817 ρ_i, and 16 particles per cell. Convergence tests indicated that higher parallel resolution was needed for the noncircular case than for the corresponding circularized cases, primarily because of the somewhat sharper variation of the local magnetic shear and the curvature components as a function of poloidal angle.

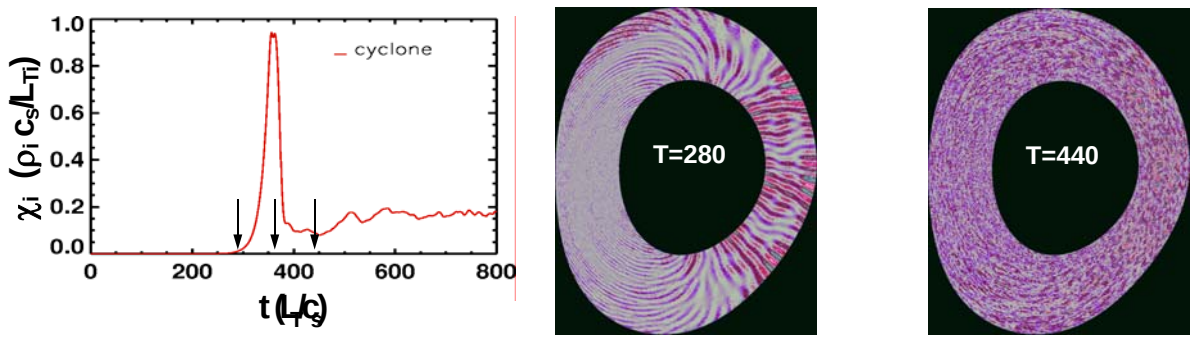

Figure 4. Time history of χ_i and images of the electrostatic potential in a poloidal section from a PG3EQ_NC simulation using a real DIII-D equilibrium from EFIT and ONETWO analyses of shot #81499 at t=4000ms, and r/a=0.509. The times in the simulation are t=280 and 440 L_{Ti}/c_s.

Figure 5 shows the maximum growth rate versus minor radius from PG3EQ_NC simulations using the equilibria from EFIT and ONETWO analyses and circularized equilibria for DIII-D shots (a) #81499 at t=4000ms and (b) #118561 at t=1450ms.

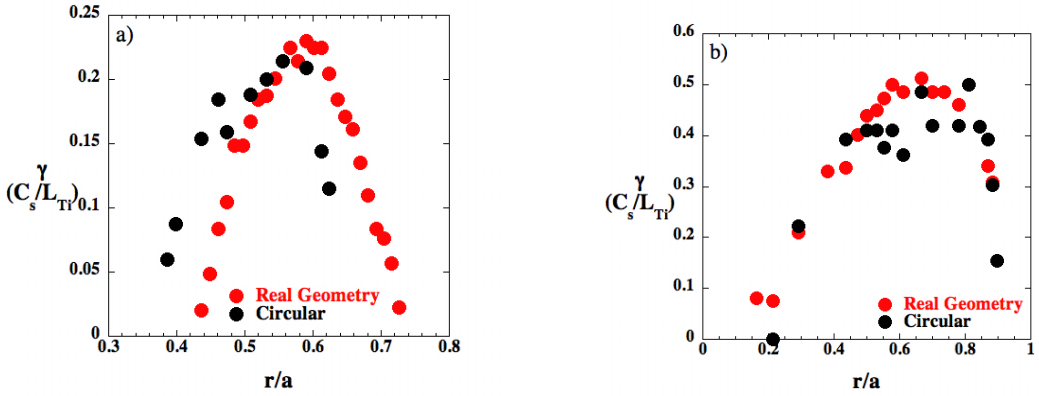

Figure 5. Maximum ITG growth rates (in units of c_s/L_{Ti}) vs. minor radius from PG3EQ_NC simulations using real DIII-D equilibria (red) and circularized equilibria (black) from (a) shot #81499 at t=4000ms and (b) shot #118561 at t=1450ms.

The shot #81499 cases show a modest effect of shaping, with the real-geometry $\gamma(r)$ profile shifted slightly outwards relative to the circular case. The shot #118561 cases show very little effect from shaping. Examination of the local equilibrium parameters indicates that the toroidal ITG modes become stable at large minor radius primarily because the magnetic shear becomes large. At small minor radius, the growth rates become small because the temperature gradient becomes small causing the dimensionless parameters R/L_{Ti} and $\eta_i=L_{ni}/L_{Ti}$ to fall below marginal values.

Presently being undertaken are (1) a comparison of these $\gamma(r)$ profiles with results from the GKS code [30], and (2) larger nonlinear simulation runs for that will yield χ_i profiles for both of the discharges studied here.

5. Summary and conclusions.

We have reported progress on understanding gyrokinetic of electron- and ion-temperature-gradient (ETG and ITG) turbulence [3,4].

We have carried out an investigation, using both PIC and continuum simulations as well as analytical theory, of the discrepancy between previous continuum-code [1] and global-PIC [2] gyrokinetic simulations of ETG turbulence. This investigation strongly supports the conclusions of the earlier continuum-code simulations, that levels of the electron thermal conductivity χ_e are large enough to be significant in some tokamaks.

A successful benchmark between PIC and continuum codes for ETG turbulence has been completed. Because both PIC- and continuum-code ETG simulations at the plasma parameters used above produce very large intermittent transport and strong sensitivity of the results to numerical parameters, this benchmarks was undertaken at an alternate reference point, magnetic shear s=0.1 instead of s=0.796. At this more tractable benchmark point, good agreement was achieved, with the time-interval weighted standard deviation in $\langle\chi_e\rangle$ between codes yielding an error in our estimate of the mean of less than 10%. This agreement between codes is better than that achieved in the Cyclone ITG benchmarking exercise [13].

Scans in the magnetic shear show an abrupt transition to a high-χ_e state as the shear is increased above s=0.4, and good agreement between codes in tracking this trend. When nonadiabatic ions are used, this abrupt transition is absent, and χ_e increases gradually reaching values consistent with transport analyses of DIII-D, JET, and JT60-U discharges.

The balances of zonal-flow driving and damping terms in late-time quasi-steady phase have been unfolded using a new run-time gyrokinetic-simulation diagnostic that we have developed. This investigation contrasts with most previous zonal-flow generation and damping studies, which mostly addressed either the early-time onset of the zonal flows or looked at otherwise transient behavior evolving from a simplified initial state. This investigation is important because zonal flows play a key role in regulating toroidal ITG turbulence and transport. The driving of the zonal flows in this phase was found to be mostly by the Reynolds' stress, while the dissipation is mostly by the linear (transit-time) damping terms. An issue affecting the viability of applying such a diagnostic directly to experimental data has been addressed by showing that in the simulations, useful zonal-flow-balance information can be obtained with spatially localized samples at as few as four poloidal locations.

Finally, studies of the effect of real geometry on ITG turbulence using SUMMIT/PG3EQ_NC, a real-geometry version of our nonlinear δf-PIC gyrokinetic code PG3EQ, were reported. Real DIII-D equilibrium reconstruction data from EFIT, ONETWO, and PLOTEQ-code analyses are used. Shots addressed include the DIII-D "Cyclone" shot #81499, and shot #118561. The former shot was the basis for earlier ITG benchmarks. In the latter, plasma instabilities were excited by using short duration neutral beam blips to modify the plasma parameters, and were diagnosed using broad wavenumber range density fluctuation measurements. The simulations completed so far show modest effects of real geometry on the maximum linear growth rate profiles, but some reduction in the thermal transport levels in the late-time nonlinear state compared with the circularized cases.

Acknowledgments: We would like to thank the following for useful discussions: B. Cohen, K. Hallatschek , W. W. Lee, Z. Lin, S. Parker, B. Scott, E. J. Synakowski, M. Umansky, X. Q. Xu., as well as H. St. John for his help with the PLOTEQ code. This work performed for US DOE at U.C. LLNL under Contract No. W-7405-ENG-48, at PPPL under Contr. No. DE-AC02-76CH03073, U. Maryland under Grant No. DE-FG02-93ER54197, UCLA under Grant No. DE-FG02-04ER54740, and at General Atomics under contract Nos. DE-FG03-95ER54309 and DE-FG02-92ER54141. Some of the simulations described here made use of resources at the National Energy Research Supercomputer Center under Department of Energy Contract No. DE-AC03-76SF00098.

References:

[1] Jenko F Dorland W Kotschenreuther M and Rogers B N 2000 *Phys. Plasmas* **7**, 1904
Dorland W Jenko F Kotschenreuther M and Rogers B N 2000 *Phys. Rev. Lett.* **85**, 5570

[2] Lin Z Chen L Nishimura Y Qu H Hahm *et al.* 2005 Electron Thermal transport in Tokamaks: ETG or TEM Turbulence? *Proc. 20th Fusion Energy Conference, Vilamoura, 2004* (IAEA, Vienna,) paper TH8_4 (see http://www-naweb.iaea.org/napc/physics/fec/fec2004/datasets/index.html) Lin Z *et al.* 2005 Phys. Plasmas **12** 056125

[3] Nevins W M Hammett G W Dimits A M Dorland W and Shumaker D E 2005 *Phys. Plasmas* 1 122305

[4] Nevins W M Candy J Cowley S Dannert T *et al.* 2006 *Phys. Plasmas* **13** 122306

[5] Luce T C *et al.* 1995 *Proc.15th. Int. Conf. on Plasma Physics and Controlled Nuclear Fusion* (IAEA Vienna paper A-2-III-2)

[6] Hammett G W Beer M A Dorland W Cowley S C and Smith S A 1993 *Plasma Phys. Control. Fusion* **35** 973-985

[7] Dimits A M Byers J A Williams T J and Cohen B I *et al.* 1995 *Proceedings of the 15th International Conference on Plasma Physics and Controlled Nuclear Fusion Research, Seville,* (International Atomic Energy Agency, Vienna, Vol. **3** p. 457)

[8] Dimits A M Williams T J Byers J A and Cohen B I 1996 *Phys. Rev. Lett.* **77**, 71

[9] Chen L Lin Z and White R 2000 *Physics of Plasmas* **7** 3129-3132

[10] Rogers B N Dorland W and Kotschenreuther M 2000 *Phys. Rev. Lett.* **85** 5336

[11] Scott B. 2003 *Phys. Lett. A* **320** 53

[12] Hallatschek K and Zeiler A 2000 *Phys. Plasmas* **7** 2554-2564

[13] Dimits A M Bateman G Beer M A Cohen B I *et al.* 2000 *Phys. Plasmas* **7**, 969

[14] Lee W W Ethier S Jenkins T G Wang *et al.* 2006 Long Time Simulation of Microturbulence in *Proc. 21st Fusion Energy Conference* Chengdu paper TH2_6Rb (See http://www-pub.iaea.org/MTCD/Meetings/FEC2006Presentations/Presentations/17-oct-06/talk_TH2-6Ra.pdf and http://www-pub.iaea.org/MTCD/Meetings/FEC2006/th_2-6rb.pdf)

[15] Krommes 1993 J A *Phys. Fluids* B **5** 1066

[16] Candy J and Waltz R E 2003 *J. Comput. Phys.* **186** 545

[17] Candy J and Waltz R E 2006 Coupled ITG/TEM-ETG Gyrokinetic Simulations *Proc. 21st Fusion Energy Conference* Chengdu paper TH2_6Rb (http://www-pub.iaea.org/MTCD/Meetings/FEC2006/th_2-1.pdf and http://www-pub.iaea.org/MTCD/Meetings/FEC2006Presentations/Presentations/17-oct-06/Talk_TH2-1/Talk_TH2-1.pdf)

[18] Stallard B W Greenfield C M Staebler G M Rettig *et al.* 1999 *Phys. Plasmas* **6**, 1978

[19] Parail V V Baranov Yu F Challis C D Cottrell G A *et al.* 1999 *Nucl. Fusion* **39**, 429

[20] Shirai H Kikuchi M Takizuka T Fujita T *et al.* 1999 *Nucl. Fusion* **39**, 1713

[21] LeBlanc B P Bell R E Kaye S M Stutman D *et al.* 2004 *Nucl. Fusion* 44, 513

[22] Braginskii S I 1965 Transport Properties in a Plasma in *Reviews of Plasma Physics* (Leontovich M A (ed.) Consultants Bureau, New York, Vol. **1**, p. 205-311)

[23] Frieman E and Chen L 1982 *Phys. Fluids* **25** 502

[24] Horton W Estes R D and Biskamp D 1990 *Plasma Physics* **22** 663

[25] Smolyakov A I Diamond P H and Medvedev M V 2000 *Phys. Plasmas* **7** 3987

[26] Cohen B I Barnes D C Dawson J M Hammett G W *et al.* 1995 *Comp. Phys. Commun.* **87** 1

[27] Lao L L St. John H Stambaugh R D Kellman A G and Pfeiffer W 1985 *Nucl. Fusion* **25** 1611

[28] Pfeiffer W W Davidson R H Miller R W and Waltz R E 1980 ONETWO: A Computer Code for Modeling Plasma Transport in Tokamaks (General Atomics Report GA-A16178).

[29] St. John H. 2004 (Private Communication)

[30] Kotschenreuther M Rewoldt G and Tang W M 1995 *Comp. Phys. Comm.* **88** 128